16th ICAAR LISBOA 2020-2022

16th International Conference on
Alkali-Aggregate Reaction in Concrete
Lisboa | LNEC | Portugal | 31 May - 2 June 2022

http://icaar2020-2022.lnec.pt

Shear capacity of RC beams damaged by combined deterioration due to ASR and corrosion

Yasuhiro Mikata [(1)], Ryota Matoba [(2)], Taijyu Ura [(3)], Takayuki Fumoto [(4)]

(1) Osaka Institute of Technology, Osaka, Japan, yasuhiro.mikata@oit.ac.jp

(2) Farmer, Wakayama, Japan

(3) Kintetsu Railway Co., Ltd., Osaka, Japan

(4) Kindai University, Osaka, Japan

Abstract

Instances of reinforcing steel fracture in concrete structures damaged by the alkali-silica reaction (ASR) have been discovered recently. When many steel bars are fractured, strengthening is often required because of possible overloading caused by the reduced performance of the member or structure due to ASR-induced cracking. It is thus important to clarify the residual performance of the loading capacity of RC (reinforced concrete) members damaged by ASR. In particular, the shear capacity of RC with reinforcing steel bar fractures is unknown. In this study, RC beams damaged by combined deterioration due to ASR and corrosion and that have steel bar fractures are tested to evaluate their shear capacity. In addition, an ultrasonic propagation velocity test and X-ray computed tomography analysis are applied to a test specimen to estimate ASR-induced cracking inside the concrete. The results show that the shear force carried by the shear reinforcement of RC beams with steel bar fractures is lower than that of the sound beam specimen. ASR-induced cracking is found to progress gradually inside the concrete, as determined from X-ray computed tomography analysis.

***Keywords**: fractured reinforcement; combined deterioration; shear capacity; ultrasonic propagation velocity; X-ray computed tomography (CT)*

1. INTRODUCTION

Instances of reinforcing steel fracture in concrete structures damaged by the alkali-silica reaction (ASR) have been discovered recently. Japan currently has about 30 ASR-damaged structures, including highway and railroad bridges, confirmed to have steel bar fractures. In addition, combined deterioration due to ASR and corrosion has been confirmed in some bridges [1]. The safety of these structures is considered to be not seriously compromised. However, safety becomes questionable when the cross-sectional areas of reinforcements decrease due to corrosion [2,3]. When many steel bars are fractured, strengthening is often required because of possible overloading caused by the reduced performance of the member or structure due to decreased concrete strength and Young's modulus. It is thus important to clarify the residual performance of the loading capacity of RC members damaged by ASR and corrosion. In particular, the shear capacity of RC with reinforcing steel bar fractures is unknown. In this study, RC beams damaged by combined deterioration due to ASR and corrosion and that have steel bar fractures are tested to evaluate their shear capacity.

When estimating the soundness of RC members damaged by ASR, ultrasonic propagation velocity is used, however, the influence of the ASR-induced cracking inside the concrete for the ultrasonic propagation velocity is not known. An ultrasonic propagation velocity test and X-ray computed tomography (CT) analysis are applied to a test specimen to estimate. The test specimen was made of the same concrete as that of the beam specimen.

2. MEASUREMENT AND TEST METHOD

2.1 Test method for beam specimens

As shown in Figure 2.1, the test specimens were simple RC beams with a rectangular cross section of 100 mm × 200 mm and a total length of 1800 mm.

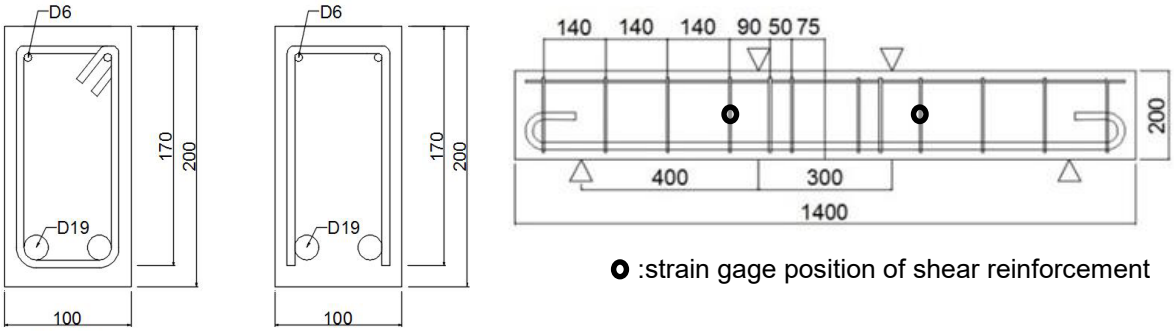

(a) Cross section (Sound stirrup) (b) Cross section (Fractured anchorage) (c) Side view of specimens

Figure 2.1: Dimensions of RC beam specimens (unit: mm)

Three types of deterioration were considered, namely ASR (A series specimens), combined deterioration due to ASR and corrosion (AC series specimens), and sound (N series specimens). To evaluate the effect of the shear force carried by shear reinforcement due to steel bar fractures, two types of specimen, namely those with a sound stirrup and those with a fractured anchorage of the shear reinforcement, were fabricated.

The main reinforcement was 2-D19 (SD345). The shear reinforcement was D6 (SD345). The spacing of shear reinforcements was 140 mm (shear reinforcement ratio ρ_w = 0.45%). All specimens were cured for 4 weeks under normal moist-curing at 20 °C. The N series specimens were placed in a constant-temperature and humidity chamber to maintain room temperature (20 °C) and high humidity (90%).

The A series specimens were cured for 4 weeks and then placed in a constant-temperature and -humidity chamber to be subjected to ASR under high-temperature (40 °C) and high-humidity (90%) conditions. The AC series specimens were cured for 4 weeks and then placed in a constant-temperature and -humidity chamber to be subjected to ASR under high-temperature (40 °C) and high-humidity (90%) conditions and was sprayed with 3% saline water to promote combined deterioration.

Table 2.1: Mix proportion of concrete[1]

Series	Mix proportion	Specimen[2]	Unit weight (kg/m^3)								
			W	C	S[3]		G[4]		$NaNO_2$	NaCl	A[5] (g)
					S_n	S_r	G_n	G_r			
N	1	Beams, CT	183	290	791	0	988	0	0	0	725
A	2	Beams	183	290	807	0	494	492	15.6	0	725
	3	Beams	183	290	399	412	494	492	15.6	0	725
AC	2	Beams, CT	183	290	807	0	494	492	0	13.1	725
	3	Beams	183	290	399	412	494	492	0	13.1	725

[1] G_{max} = 20 mm, slump: 8 cm, W/C = 63%, Air = 4%, s/a = 45.8%

[2] CT: Cylinder test specimen was observed using X-ray computed tomography analysis.

[3] S_n: normal fine aggregate, S_r: reactive fine aggregate

[4] G_n: normal coarse aggregate, G_r: reactive coarse aggregate

[5] A: air-entraining and water-reducing admixture

Table 2.2: Details of test specimens

Series	Specimen	Concrete type	Anchorage of shear reinforcement[1]	Mix proportion[2]
N	N-1-14	Sound	S	1
	N-2-14		F	1
	N-1-15		S	1
	N-2-15		F	1
A	A-1-14	ASR	S	2
	A-2-14		F	2
	A-1-15		S	3
	A-2-15		F	3
AC	AC-1-14	ASR+ corrosion	S	2
	AC-2-14		F	2
	AC-1-15		S	3
	AC-2-15		F	3

[1] S: sound, F: fractured anchorage

[2] Type 1 (normal concrete), type 2 (only reactive coarse aggregate), type 3 (reactive fine aggregate and reactive coarse aggregate)

The mix proportion of concrete is shown in Table 2.1. Details of the test specimens are shown in Table 2.2. For the A and AC series specimens, 15.6kg/m^3 of $NaNO_2$ and 13.1kg/m^3 of NaCl, which had an alkali amount equivalent to 7.0kg/m^3 of Na_2O, was added to promote ASR. The main reactive components identified from the texture of andesite crushed stone were volcanic glass, cristobalite, and tridymite.

2.2 Measurements of ASR expansion

A contact gauge tip was attached to both sides of the test specimens and beam specimens to measure ASR expansion, which was evaluated as free expansion without reinforcement. The ASR expansion strains of the beam specimens were measured at the surface concrete at the position of longitudinal reinforcement (length of extreme compression fiber of the section: 170 mm).

2.3 Measurements of corrosion

The ratio of corrosion weight loss was calculated from the sound (original) weight of the reinforcement and the corrosion weight loss across the overall length. The sound (original) weight of the reinforcement was obtained by measuring the reinforcement alone (i.e., before the RC beam was cast). The corrosion weight loss was measured by removing the rust of the corroded longitudinal reinforcement, which was taken out of the RC beam after the loading test, using a 10% di-ammonium hydrogen citrate solution at 60 °C.

2.4 Loading test

All specimens were tested under symmetrical two-point loads with a flexural span of 300 mm and a shear span of 400 mm. The shear span/effective depth ratio of these beams was a/d = 2.35. The displacement was measured at the deflection of the center of the beam specimen under the loading test.

2.5 Non-destructive test of cylindrical specimen

X-ray CT analysis was applied to a cylindrical test specimen to estimate ASR-induced cracking inside the concrete. In addition, an ultrasonic propagation velocity test was conducted and its results were compared with those of the X-ray CT analysis. Two types of deterioration were considered, namely ASR

(A-CT series specimens) and sound (N-CT series specimens). The A-CT and N series specimens were fabricated using mix proportion types 2 and 1, respectively. Figure 2.2 shows the X-ray CT scanner [4]. Scanning was carried out with a tube voltage of 220 kV and a tube current of 100 μA. A range of 100 mm in diameter and 50 mm in height was scanned in one shot. A test specimen with a diameter of 100 mm and a height of 200 mm was scanned in four shots. The CT scanner produced cubic isotropic voxels with a size of 0.123 mm. The opacity of each voxel was represented by an 8-bit gray-scale value. Continuous isometric CT scans were acquired to reconstruct three-dimensional images. Cracks and voids were displayed as gray to black depending on their width. A crack with a width of about 0.1 mm could be observed.

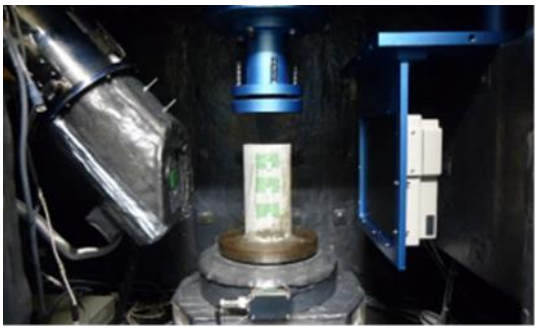

Figure 2.2: Photograph of X-ray CT scanner

3. RESULTS AND DISCUSSION FOR BEAM SPECIMENS

3.1 ASR expansion

Figure 3.1 shows the axial strain of ASR expansion for the A and AC series beam specimens. The ASR expansion strains of A-1-14 and AC-1-14 were about 250×10^{-6} and 320×10^{-6} at 400 days, respectively. Those of A-1-15 and AC-1-15 were about 400×10^{-6} and 450×10^{-6} at 320 days, respectively. The ASR expansion strains of A-1-15 and AC-1-15 are larger than those of A-1-14 and AC-1-14 because A-1-15 and AC-1-15 were made with mix proportion type 3, which had the reactive fine aggregate and the reactive coarse aggregate, whereas A-1-14 and AC-1-14 were made with mix proportion type 2, which had only the reactive coarse aggregate.

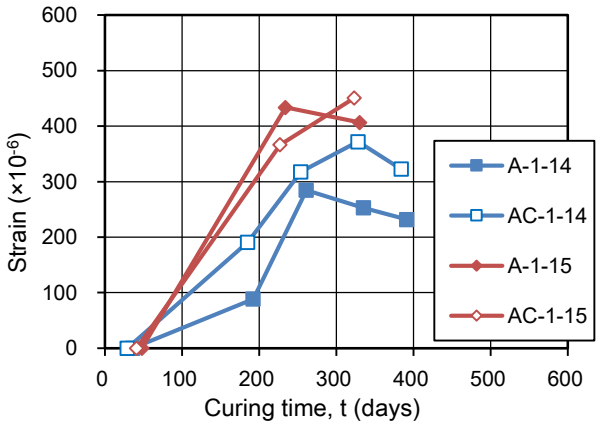

Figure 3.1: Axial strain of ASR expansion

3.2 Crack conditions

Figure 3.2 shows the crack conditions before the loading tests. For the A series specimens, ASR-induced cracks formed in the whole area except at the position of longitudinal reinforcement. The top surface of the specimens had the most cracks. Because there were few confinements by reinforcements compared with the other surface. For the AC series specimens, both ASR- and corrosion-induced cracks

formed. The corrosion-induced cracks formed in the surface concrete at the position of longitudinal reinforcement due to the corrosion of the reinforcement. Most cracks had a width of over 0.2 mm.

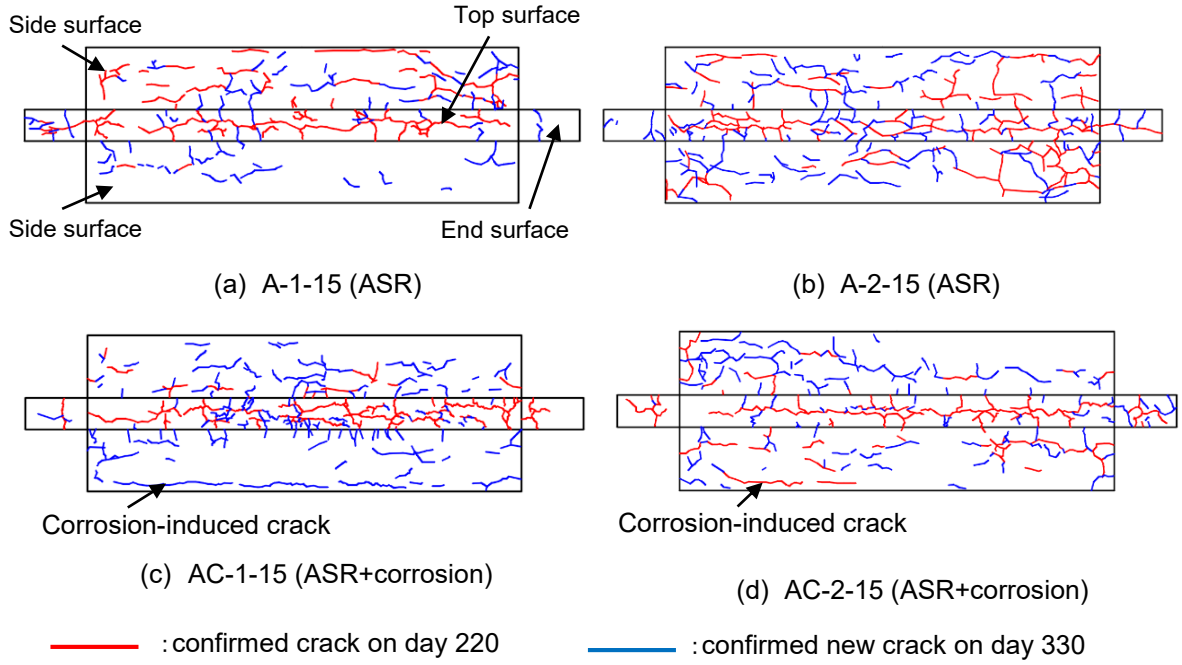

Figure 3.2: Crack conditions before loading tests

3.3 Measurements of corrosion

The mechanical properties of the corroded reinforcing bars are listed in Table 3.1. The corroded longitudinal reinforcement was taken out of the RC beam after the loading test. The yield strength and elastic modulus were calculated from experimental values using the nominal cross-sectional area. The ratios of corrosion weight loss were 0.48% to 1.20%.

Table 3.1: Mechanical properties of corroded reinforcing bars

Specimen	Ratio of corrosion weight loss (%)	Yield strength (N/mm^2)	Elastic modulus (kN/mm^2)
AC-1-14	0.59	389.1	197.5
AC-2-14	0.48	390.4	199.7
AC-1-15	1.06	376.3	195.2
AC-2-15	1.20	370.3	192.1

3.4 Properties of concrete

The properties of concrete are listed in Table 3.2. The elastic modulus values for the A and AC series specimens on the day of the loading test were lower than those on day 28 due to ASR-induced cracks.

3.5 Failure mode

Figure 3.3 shows the final failure mode. The results of loading tests are listed in Table 3.3. Figure 3.4 shows the relationship between load and displacement. Figure 3.5 shows the shear reinforcement strain of ASR expansion. Figure 3.6 shows the relationship between load and shear reinforcement strain. N-2-15 showed shear tension failure. A shear crack formed along the longitudinal reinforcement from the center of the shear span to the support points. This specimen had a fractured anchorage of the shear reinforcement. The confinement force of the dowel action of the longitudinal reinforcements

decreased due to this fractured anchorage. Therefore, a shear crack formed along the longitudinal reinforcement. A-1-15 and AC-1-15 showed flexural tension failure. Shear cracks formed at both or one side of the shear span.

Table 3.2: Properties of concrete

Specimen	Compressive strength (N/mm^2)		Elastic modulus (kN/mm^2)		Concrete age during loading test (days)
	Day 28	Loading test day	Day 28	Loading test day	
N-1-14 N-2-14	18.7	18.7	25.2	25.2	399
A-1-14 A-2-14	13.6	17.8	21.0	18.6	406
AC-1-14 AC-2-14	19.1	19.2	25.9	25.8	405
N-1-15 N-2-15	25.8	40.3	28.8	35.9	356
A-1-15 A-2-15	24.8	24.1	28.9	10.3	357
AC-1-15 AC-2-15	22.2	17.7	24.1	10.9	350

Table 3.3: Results of loading tests

Specimen	Ultimate load capacity (mea.), P_u (kN)	Ultimate flexural capacity[1] (cal.), P_{ub} (kN)	Ultimate shear capacity (cal.)		Shear force carried by concrete[2], Vc (kN)	Shear force carried by shear reinforcement[2], Vs (kN)	Failure mode[3]
			P_{us} (=2×Vy) (kN)	Vy (=Vc+Vs) (kN)			
N-1-14	159	109	102	50.8	20.3	30.5	SC
N-2-14	166	109	102	50.8	20.3	30.5	ST
A-1-14	118	105	101	50.5	20.0	30.5	DT
A-2-14	112	105	101	50.5	20.0	30.5	DT
AC-1-14	146	111	102	51.0	20.5	30.5	DT
AC-2-14	118	111	102	51.0	20.5	30.5	DT
N-1-15	176	150	113	56.7	26.2	30.5	DT
N-2-15	137	150	113	56.7	26.2	30.5	ST
A-1-15	164	124	105	52.6	22.1	30.5	FT
A-2-15	144	126	105	52.6	22.1	30.5	DT
AC-1-15	169	104	101	50.4	19.9	30.5	FT
AC-2-15	141	103	101	50.4	19.9	30.5	DT

[1] Values caluculated using fiber model

[2] Calculated shear capacity based on JSCE standard specification

[3] SC: shear compression failure, ST: shear tension failure, DT: diagonal tension failure, FT: flexural tension failure

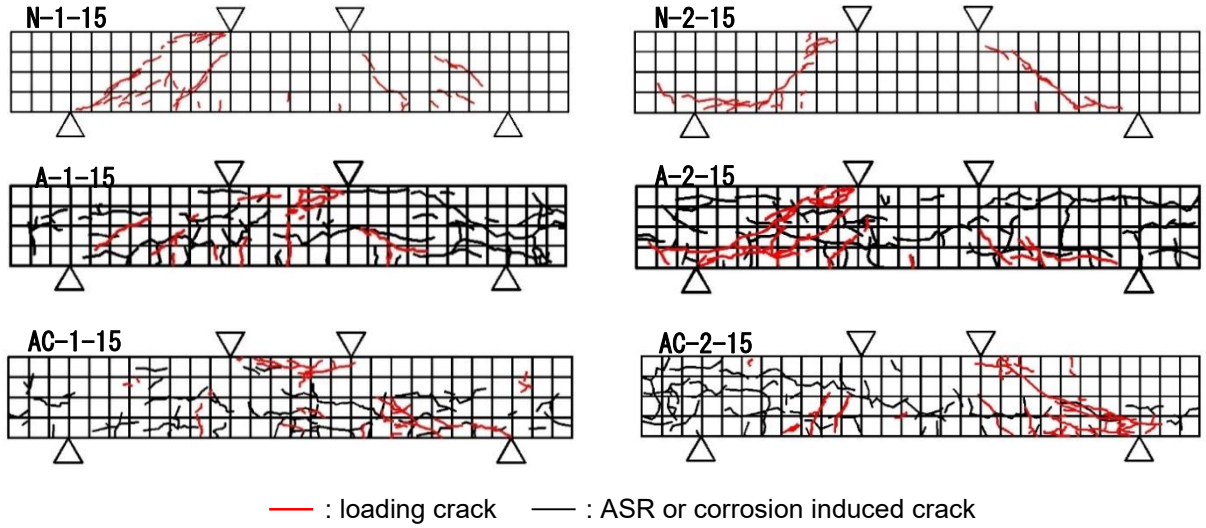

Figure 3.3: Final failure modes

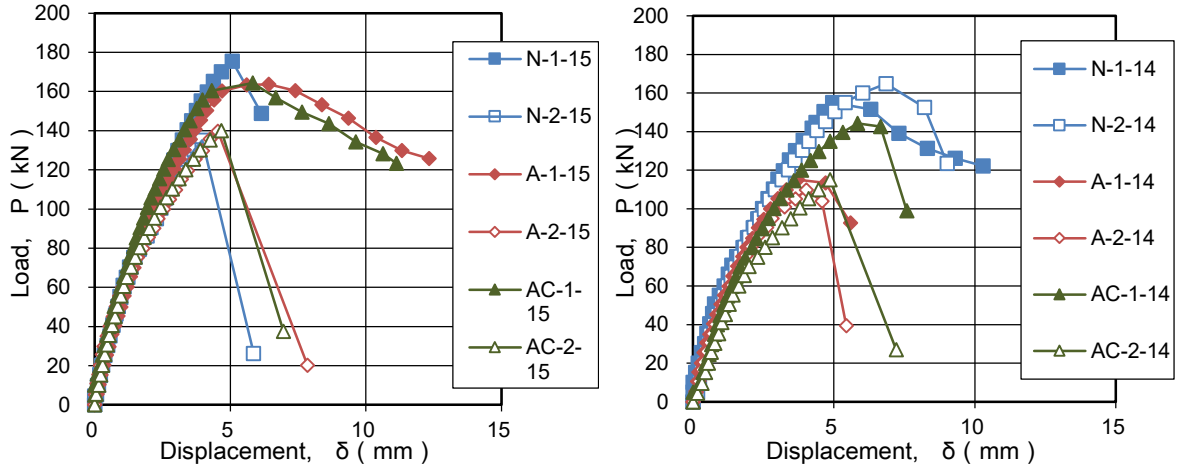

Figure 3.4: Relationship between load and displacement

However, these cracks did not expand to the loading or support point. These specimens showed compressive failure in the flexural span.A-2-15 and AC-2-15 showed diagonal tension failure. When a shear crack connected to an ASR- or corrosion-induced crack at the position of the longitudinal reinforcement, the crack width increased. These specimens failed due to the expansion of the shear crack from the loading point to the support point. For A-2-15 and AC-2-15, the ultimate load was lower than that of A-1-15 and AC-1-15. In addition, the failure mode was different from those for A-1-15 and AC-1-15. The confinement performance of the shear reinforcement decreased due to the fractured anchorage. In addition, the chemical prestress carried by the shear reinforcement decreased due to the fractured anchorage. Therefore, A-2-15 and AC-2-15 showed diagonal tension failure. For the A and AC series specimens, the shear stress was complicated due to the connection of the shear crack to an ASR- or corrosion-induced crack. AC series specimens have not caused a clear difference with A series specimens because corrosion of reinforcing bars was slight.

After shear crack occurred, the shear reinforcement strain of each specimen has increased. On one hand, maximum strain of N-1-15 are about 2000×10^{-6}. On the other hand, maximum strain of N-2-15 are about 1700×10^{-6}. Strain of N-2-15 are smaller than that of N-1-15 due to the fractured anchorage of shear reinforcement. On one hand, maximum strain of AC-1-15 are about 1200×10^{-6}. On the other hand, maximum strain of AC-2-15 are about 1000×10^{-6}. Strain of AC-2-15 are smaller than that of AC-1-15 due to the fractured anchorage of shear reinforcement. Before loading test, the shear reinforcement strain of AC-1-15 are about 1860×10^{-6} at 320days due to ASR expansion.

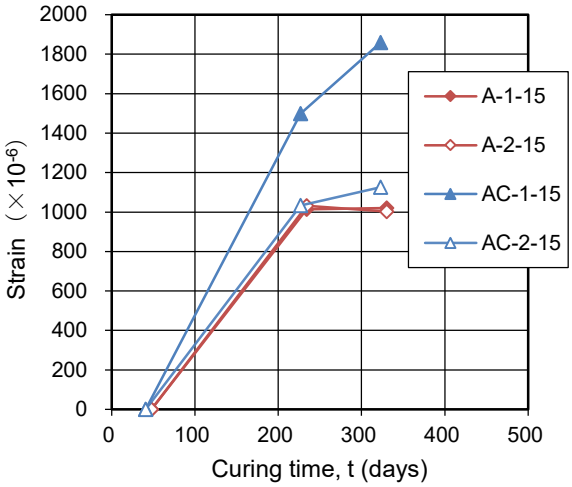

Figure 3.5: shear reinforcement strain of ASR expansion

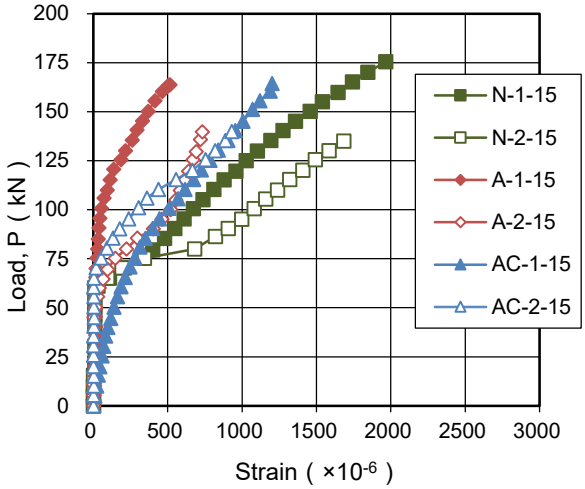

Figure 3.6: Relationship between load and shear reinforcement strain

The yield strain of shear reinforcement was 2250×10^{-6}. Most strain to yield point of shear reinforcement was consumed by ASR expansion. Therefore, shear force carried by shear reinforcement seems to be reduced in the loading test.

4. RESULTS AND DISCUSSION FOR CYLINDRICAL SPECIMENS

4.1 Ultrasonic propagation velocity test

Figure 4.1 shows the ultrasonic propagation velocity results, where N and N-CT average values for three sound specimens in the compressive test and X-ray computed tomography test, respectively, and A and A-CT average values of three ASR specimens in the compressive test and X-ray compressive test, respectively. A-CT-1 is an ASR specimen in the X-ray compressive test. The ultrasonic propagation velocities of A and A-CT on day 483 were 36% and 19% lower than those on day 28, respectively. Those of N and N-CT did not change.

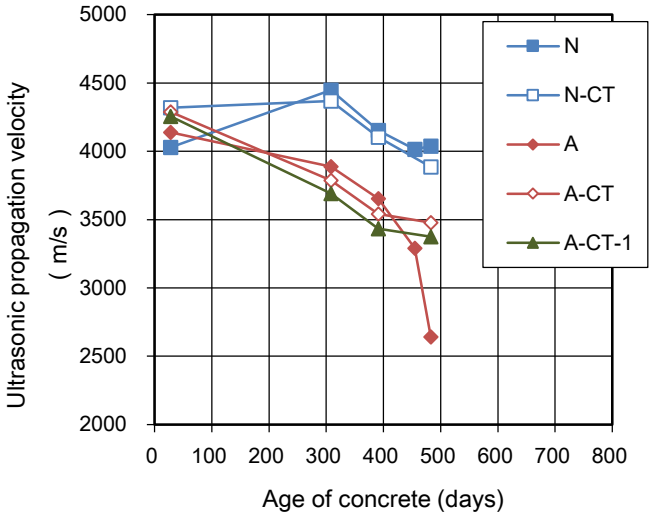

Figure 4.1: Ultrasonic propagation velocity

4.2 X-ray computed tomography analysis

Figure 4.2, Figure 4.3, and Figure 4.4 show CT image slices through the A-CT-1 specimen on days 28, 308, and 483, respectively. The CT images are the cross section at 100 mm from the top face of the cylindrical specimen. The crack widths are indicated in the CT image.

The ASR-induced crack had not yet formed on day 28. However, a 0.2-mm-wide crack formed inside the aggregate at 308 days. The ultrasonic propagation velocity of A-CT-1 on day 308 was 13% lower than that on day 28. Another crack formed inside the same aggregate on day 483. The original 0.2-mm-wide crack widened to 0.3 mm on day 483. Other cracks formed inside other aggregates. The ultrasonic propagation velocity of A-CT-1 on day 483 was 21% lower than that on day 28.

The CT images show a certain cross section whereas the ultrasonic propagation velocity was measured from the top to bottom of the cylinder. If all cracks in the cylinder can be detected by X-ray CT analysis, this analysis can be used to evaluate the ultrasonic propagation velocity. In addition, cracks inside the aggregate could be detected in the CT images. CT images can thus be used to determine the mechanism of crack formation inside the aggregate.

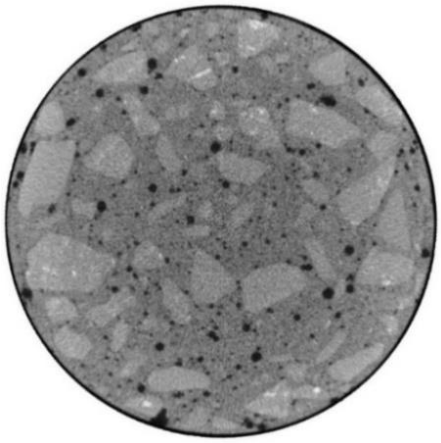

Figure 4.2: CT image at 28 days

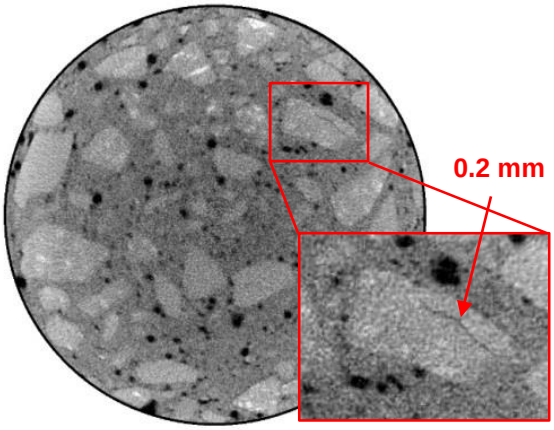

Figure 4.3: CT image at 308 days

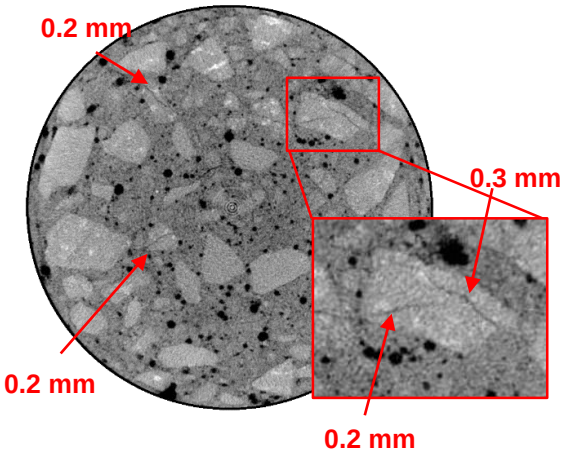

Figure 4.4: CT image at 483 days

5. CONCLUSION

The main conclusions obtained in this study are as follows:

(1) For the A series specimens, ASR-induced cracks formed in whole area except at the position of the longitudinal reinforcement of specimens. The top surface of the specimens had the most cracks. Because there were few confinements by reinforcements compared with the other surface. For the AC series specimens, both ASR- and corrosion-induced cracks formed. The corrosion-induced cracks formed in the surface concrete at the position of the longitudinal reinforcement due to the corrosion of the reinforcement.

(2) For A-2-15 and AC-2-15, the ultimate load was lower than that for A-1-15 and AC-1-15. In addition, the failure mode was different from that for A-1-15 and AC-1-15. The confinement performance of the shear reinforcement decreased due to a fractured anchorage. In addition, the chemical prestress carried by the shear reinforcement decreased due to this fractured anchorage. Therefore, A-2-15 and AC-2-15 showed diagonal tension failure. For the A and AC series specimens, shear stress was complicated due to the connection of a shear crack to an ASR- or corrosion-induced crack. Before loading test, the shear reinforcement strain of AC-1-15 are about 1800×10^{-6} at 320days due to ASR expansion. Most strain to yield point of shear reinforcement was consumed by ASR expansion. Therefore, shear force carried by shear reinforcement seems to be reduced in the loading test.
(3) If all cracks in a cylinder can be detected by X-ray CT analysis, this analysis can be used to evaluate the ultrasonic propagation velocity. In addition, cracks inside the aggregate were detect in CT images, which can thus be used to determine the mechanism of crack formation inside the aggregate.

6. ACKNOWLEDGMENTS

This work was supported by ABE NIKKO KOGYO Co., Ltd. and JSPS KAKENHI Grant Number JP17K06522.

7. REFERENCES

[1] Japan concrete institute (1998) Technical Committee on Evaluation of Combined Deterioration on Concrete Structures and Its Maintenance Planning (in Japanese)

[2] Mikata,Y., Fukutani, S., Tanaka, H. and Inoue, S. (2015) Effect of Combined Deterioration due to ASR and Corrosion on Loading Capacity of RC Beams , Proceeding of the International Conference on the Regeneration and Conservation of Concrete Structures, Nagasaki, Japan, JCI

[3] Mikata, Y., Shimazu, Y., Hatano, Y. and Inoue, S. (2012) Flexural and shear capacity of PRC beams damaged by combined deterioration due to ASR and corrosion, Proceedings of the 14th International Conference on Alkali-Aggregate Reaction in concrete, Austin, U.S.A., ICAAR

[4] Fumoto, T. (2013) Development of A New Industrial X-Ray CT System and Its Application to Compression Test of Polymer Concrete (2013), Journal of materials, concrete structures and pavements, E2, V-69, No.2, pp.183-191, Japan Society of Civil Engineers (in Japanese)